Phys. Status Solidi C **13**, No. 10–12, 932–936 (2016) / **DOI** 10.1002/pssc.201600081

physica status solidi c
www.pss-c.com
current topics in solid state physics

Charged oxygen interstitials in corundum: first principles simulations

Alexander Platonenko[*], Denis Gryaznov[**], Sergei Piskunov[***], Yuri F. Zhukovskii[****], and Eugene A. Kotomin[*****]

Institute of Solid State Physics, University of Latvia, 8 Kengaraga, 1063 Riga, Latvia

Received 31 May 2016, revised 12 July 2016, accepted 18 July 2016
Published online 9 August 2016

Keywords corundum, defects, oxygen interstitial, diffusion, first principles calculations

[*] Corresponding author: e-mail alexander.platonenko@gmail.com, Phone: +371-25956583, Fax: +371-67132778
[**] e-mail gryaznov@mail.com, Phone: +371-27434516, Fax: +371-67132778
[***] e-mail piskunov@lu.lv, Phone: +371-20093610, Fax: +371-67132778
[****] e-mail quantzh@latnet.lv, Phone: +371-28824271, Fax: +371-67132778
[*****] e-mail kotomin@latnet.lv, Phone: +371-6718 7480, Fax: +371-67132778

Combining supercell models and hybrid B3PW exchange-correlation functionals, *ab initio* simulations on quasi-stable configurations of interstitial O_i^- ions in α-Al_2O_3 (corundum) crystals and possible migration trajectories have been modelled. We have studied crystalline distortion around migrating O_i^- including interatomic distances and the effective atomic charges, as well as redistributions of the electronic density. Unlike neutral interstitial atom O_i studied by us previously, migrating O_i^- ion does not form dumbbells with the nearest regular O_{reg}^{q-} oxygen ions, due to the strong Coulomb interaction with the nearest Al_{reg}^{q+} cations as well as stronger repulsion between O_i^- and adjacent regular O_{reg}^{q-} ions. We have also estimated the energy barrier for migration between the nearest quasi-stable configurations of interstitial O_i^- ion. One of these configurations is an octahedron formed by six nearest O_{reg}^{q-} anions in the centre of which O_i^- ion is located, unlike a neutral O_i atom which prefers to migrate directly towards one of adjacent O_{reg}^{q-} anions with the dumbbell formation. As the result, the barrier for O_i^- ion migration in corundum has been found to be by ~70% smaller than that of O_i atom.

1 Introduction Various types of point defects created by irradiation of α-Al_2O_3 (corundum) by high-energy neutrons and ions have been intensively studied during last two decades, both experimentally and theoretically [1-14]. Structural changes as a result of exposure to radiation appear mainly as neutral and charged aluminium and oxygen vacancies (V_{Al} and V_O) [1-8, 11, 14], interstitial atoms (Al_i and O_i) [1, 4, 5, 7-9, 11, 12] as well as complementary Frenkel defect pairs in both sublattices: (V_{Al}+Al_i) and (V_O+O_i) [4, 7, 8, 11]. In majority of theoretical studies mentioned above, neutral point defects or Frenkel pairs have been studied, while the authors of Refs. [7, 8] analysed properties of both charged interstitials (Al_i^{q+} and O_i^{q-}) and vacancies (V_{Al}^{q-} and V_O^{q+}) as well as analogous types of neutral defects, comparing their properties. It was concluded therein that defects in their highest charge states are more stable under most conditions, but in some regimes neutral defects also exist [8].

In the two recent publications, we have reported properties of neutral Frenkel pairs (V_O+O_i) [11] and neutral O_i interstitials [11, 12]. It was found that migration of interstitial O_i atoms leads to the formation of (O_{reg}-O_i) dumbbells with regular oxygen ions. The trajectory of interstitial oxygen atom migration includes breaking its bond with one O_{reg}^{q-} ion and motion towards next-neighboring O_{reg}^{q-} ion, characterized by the energy barrier ~1.3 eV [12].

In this study, we have performed *ab initio* simulations of a charged interstitial O_i^- ion in α-Al_2O_3 using the same computational method and atomistic models as previously [11, 12], and compared the results obtained for neutral O_i atoms and charged O_i^- ions including their migration trajectories inside corundum lattice.

2 Theoretical background

2.1 Computational details Corundum crystals containing oxygen interstitials, irrespectively neutral or charged, have been calculated using DFT-LCAO method [12]. To perform spin-polarized calculations on all the defective configurations, we have applied CRYSTAL14 code [15] with localized basis set of atomic functions adapted

for periodic systems using the hybrid B3PW exchange-correlation functional [16]. Both the all-valence basis set (BS) for atomic Gaussian-type-functions (GTFs) described oxygen (constructed using pure *s*- and *d*- as well as hybrid *sp*-AOs in the form of 6*s*-2111*sp*-1*d* as described elsewhere [17]) as well as the effective core pseudopotential (ECP) DURAND-21G^* developed for Al [18] (with $3s^2 3p^1$ external valence shell) have been applied for our large-scale first principles calculations. To provide a balanced summation in direct and reciprocal lattices, the reciprocal space integration has been performed by sampling the Brillouin zone with the 4×4×4 Monkhorst-Pack mesh [19].

To perform calculations on charged defects, a uniform background charge density has been added to neutralize the charge in the reference cell [15], whereas to mimic O_i^- ion, one electron has been added to its 2*p*-orbital. The effective charges on atoms have been estimated using the Mulliken population analysis [20]. Calculations on all the defective α-Al_2O_3 structures have been performed with the defect structure optimization based on the total energy minimization [15]. The energies of the transition states (corresponding to migration barriers) have been obtained using the distinguished reaction coordinate technique following the method [21] as implemented in the CRYSTAL14 code. The optimized migration path corresponds to a trajectory of local minimum points on the potential energy surface (PES). Simulations of migration paths has been calculated in the internal coordinates, defining and freezing distance between O_i^- ion and one of the regular O_{reg}^{q-} ion on each step. The optimized structure can be identified using a "minimization" algorithm which may turn out to be either local minima or transition state (TS) structures.

2.2 Models of α-Al_2O_3 for simulations of migration paths We have used the same corundum supercells 2×2×1 (120+1 atoms) and larger 3×3×1 model (270+1 atoms) as in our recent papers [11, 12]. Figure 1 clearly shows a difference in coordination of adjacent regular Al_i^{q+} and O_{reg}^{q-} ions around one of regular oxygen ions (a), interstitial O_i atom (b) and interstitial O_i^- ion (c). All the cases could be described by different coordination numbers of regular ions surrounding considered oxygen in the centre of each image. This difference can be qualitatively explained by different charge distributions causing appearance of different local Coulomb interatomic forces.

This is why, we have selected two initial positions for interstitial oxygen (either charged or neutral): (1) oxygen is placed in the centre octahedral site (left image in Fig. 2) – O_i^- ion has been found more stable in this site due to electrostatic interaction with the nearest Al ions, and (2) interstitial oxygen atom is displaced from the center of octahedron towards one of a regular oxygen atom ($d_{O_i^0-O_{reg}} \approx$ 1.70 Å) – the dumbbell configuration. The latter has been confirmed in recent calculations [9, 12]. Nevertheless, O_i^- ion also causes an approach of a regular O_{reg}^{q-}, but closer to the center of octahedron (Fig. 1c). Majority of these calculations have been performed for a 2×2×1, although a larger 3×3×1 supercell qualitatively confirmed the same conclusions. Relying on the obtained results, we have chosen a 2×2×1 supercell for further calculations.

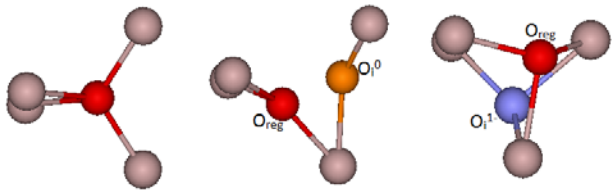

Figure 1 Reference oxygen sites in (a) perfect corundum crystal, (b) that containing neutral oxygen interstitial leading to the dumbbell formation ($d_{O_i^0-O_{reg}}$ = 1.40 Å), (c) that containing charged oxygen interstitial ($d_{O_i^- - O^{reg}}$ = 1.87 Å). All views are shown across the vertical *z*-axis (Al ions oriented along them).

Moreover, we have considered the migration path for charged oxygen interstitial from highly-symmetric point in the center of octahedral towards one of the oxygen atoms, which results in a pair configuration formation (right image in Fig. 2). On each step, O_i^- ion has been moved closer to a final site and surrounding configuration of atoms has been optimized.

3 Results and discussion

3.1 Calculations of charged oxygen interstitials According to the results obtained for both the 2×2×1 and 3×3×1 supercells, the octahedral interstitial position has been found to be less energetically favorable. After optimization interstitial oxygen does not change its position and stays in the center. For interstitial located towards regular oxygen ion, optimization has led to formation of the pair ($d_{O_i^- - O_{reg}}$ = 1.87 Å), which is energetically more favorable. The site symmetry has been preserved (Fig. 1c), so a pair consists of two equivalent oxygen atoms (Table 1). Mulliken charge analysis shows, that there is also no bond population exists between O_i^- and regular O_{reg}^{q-} ions. However, additional electron is localized within this site and involved in formation of three new O_i—Al bonds.

Table 1 Interionic distances O_i^- – Al_{reg}^{q+} ($d_{O_i\text{-}Al}$) and $O_i^- - O_{reg}^{q-}$ ($d_{O_i\text{-}O_{reg}}$) as well as the atomic effective charges in two different supercells.

supercell	$d_{O_i\text{-}Al}$, Å	$d_{O_i\text{-}O_{reg}}$, Å	effective charge, *e*		
			O_i + O_{reg}	O_{reg}	O_i
2×2×1	1.848 1.865 1.997	1.872	-1.588	-0.789	-0.789
3×3×1	1.848 1.859 2.003	1.871	-1.577	-0.788	-0.789

3.2 Migration of charged oxygen interstitial We have performed optimization of migration path between two configurations shown in Fig. 2. We observe a small energy barrier along the path, which prevents an octahedral configuration from spontaneous relaxation to a pair configuration. The barrier can be associated with the breaking of Al-O bond. It was shown earlier that diffusion of neutral oxygen interstitial does not have significant barrier. After passing the barrier, O_i^- form three Al-O bonds in total, which become stronger in the end of path. The total energy gain is 0.76 eV. This value can be considered as diffusion barrier for O_i^- interstitial migration through α-Al_2O_3 crystal, if migration path lies through centre of an octahedron.

The estimated parameters of structural relaxation of Al and O ions along the path as well as the electronic charges induced on neighbouring atoms are shown in Table 2. Interstitial O_i^- ion has a higher impact on its surrounding as compared to O_i atom. Al ions are stronger attracted to O_i^-, which results in formation of two strong Al-O_i bonds. As to regular O_{reg}^{q-} ions, they are displaced outwards O_i^-. The effective charge of oxygen interstitial increases with its motion along the path; the electronic density is mainly coming from a regular oxygen atom, which is involved in a pair formation. Thus, in the initial position interstitial oxygen has the effective charge -0.62e. During diffusion it grows to -0.73e in the transition point, and -0.79e in a final pair configuration. As a result, the total charge localized on a pair site is -1.58e and three new Al-O bonds are formed

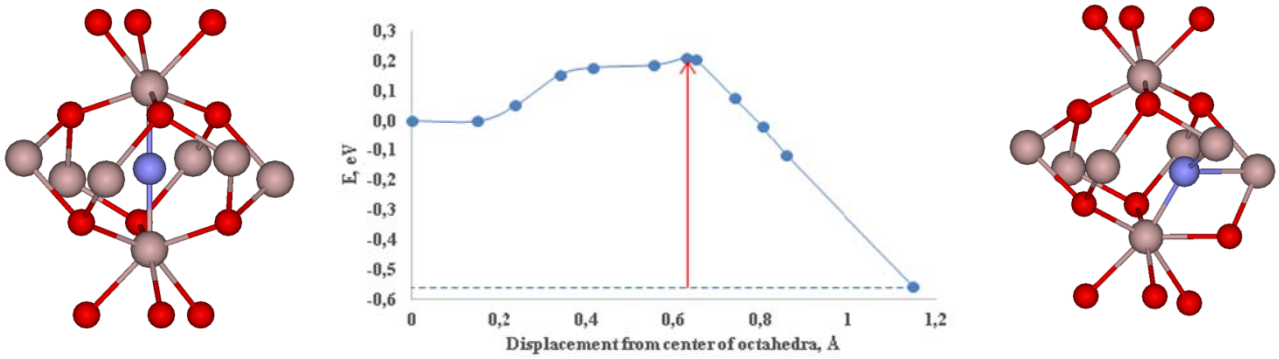

Figure 2 The energy curve for migration of interstitial O_i^- ion in corundum. Zero point corresponds to initial position in a centre of octahedron (left image), while the distance is counted from this centre to a final pair position. The height of the energy barrier is 0.76 eV.

so almost one additional electron is localized thereon (effective charges on O_{reg}^{q-} and Al_i^{q+} are -1.0e and +1.5e).

The electronic density redistribution during the migration is shown in Fig. 4. In the initial configuration (1), the additional electron is partly delocalized over a whole supercell, with a small surplus of the electronic density observed on several regular sites. In the transition configuration (2), the additional electron density is attracted from the nearest regular oxygen ions, but formation of a real covalent bond is not observed. The redistribution of the electrons on Al2 site can be associated with Al2-O_i bond breaking, which also can be one of the reasons for the migration barrier. Lastly, in a final pair configuration (3), both O_i^- and $O1_{reg}$ ions reveal the equivalent electronic configurations. Both the electronic density plots (Fig. 4) and the Mulliken population analysis (Table 2) do not show any signs of the O_i^- - O_{reg}^{q-} covalent bond formation. We suppose that the geometry of this pair is a result of the electrostatic interaction between two oxygen ions, which is energetically favourable for the formation of Al-O bonds.

Table 2 Structural relaxation of nearest ions along the migration path and their charges for initial, transition and final configurations (Fig. 3).

atoms	initial	|Δr |, Å	Δq, e	transition	|Δr |, Å	Δq, e	final	|Δr |, Å	Δq, e
Al1	1.792	0.128	0.04	1.82	0.182	0	1.85	0.24	-0.02
Al2	1.792	0.128	0.04	1.91	0.098	0	2.49	0.05	0
O1[a]	2.221	0.24	-0.05	1.95	0.340	-0.15	1.87	0.788	-0.21
O2	2.221	0.24	-0.05	2.15	0.095	-0.04	2.17	0.18	-0.02
O3	2.221	0.24	-0.05	2.23	0.115	-0.03	2.34	0.24	-0.02
Al3	2.80	0.04	0.033	2.20	0.053	0.03	1.86	0.13	0.01
Al4	2.80	0.04	0.033	2.44	0.12	0.02	2.00	0.21	-0.01
O4	3.31	0.01	0	2.80	0.078	0	2.49	0.10	0

[a] Oxygen involved in pair formation.

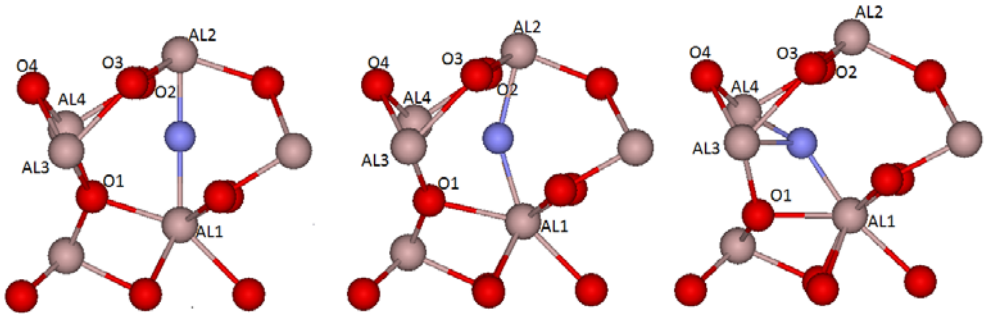

(1) (2) (3)

Figure 3 Relaxation of the nearest ions along the migration path for initial (1), transition (2) and final (3) configurations (Table 2).

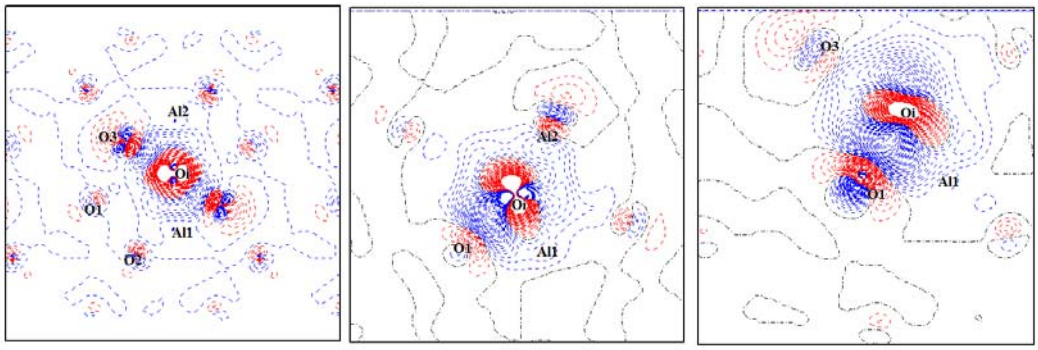

(1) Initial configuration (2) Transition state configuration (3) Pair configuration

Figure 4 2D electron density plots $\rho(\mathbf{r})$ for initial, transition and final states. Side-view planes are selected, that these planes cross oxygen interstitial as well as O_{reg}^{q-} (fully or partially). Dash-dotted (black online) isolines correspond to the zero level. Solid (red) and dashed (blue) isolines describe positive and negative values of the difference in electron density, respectively. Isodensity curves are drawn from 0.05 to +0.05 e Å^{-3} with an increment of 0.0005 e Å^{-3}.

4 Conclusions We have presented the results of large-scale *ab initio* calculations on defective corundum with radiation-induced charged interstitial O_i^- ions displaced from regular lattice sites by high-energy neutrons and ions. Unlike a neutral interstitial O_i atom, studied by us previously [11, 12], the migrating O_i^- ion does not form dumbbells with the nearest O_{reg}^{q-} ions in a corundum lattice, due to the strong Coulomb attraction to the nearest Al_i^{q+} cations and stronger repulsion from adjacent regular O_{reg}^{q-} anions.

It has been also found that one of the configurations in corundum lattice for quasi-stable location of interstitial O_i^- ion is the centre of octahedron formed by six nearest O_{reg}^{q-}

anions, unlike neutral O_i atom which prefers to migrate spontaneously from the centre of octahedron towards one of adjacent O_{reg}^{q-} anions in order to form the dumbbell configuration. As a result, the barrier for a charged O_i^- ion migration in corundum is predicted to be ~70% smaller than that for the interstitial O_i atom (0.76 eV vs. 1.30 eV [12], respectively).

Acknowledgements Authors are indebted to R.A. Evarestov, A. Lushchik, A. Popov, R. Vila for stimulating discussions. This work has been carried out within the framework of the EUROfusion Consortium and has received funding from the European Union's Horizon 2020 Research and Innovation Programme under grant agreement 633053. The views and opinions expressed herein do not necessarily reflect those of the European Commission. Support from Latvian National Research Program IMIS2 (2014–2017) and LZP Grant No. 237/2012 (2013–2016) is also appreciated. Calculations have been carried out using the HELIOS supercomputer system at Computational Simulation Centre of International Fusion Energy Research Centre (IFERC-CSC), Aomori, Japan, under the Broader Approach collaboration between Eurofusion and Japan, implemented by Fusion for Energy and JAEA.

References

[1] P.W.M. Jacobs and E.A. Kotomin, J. Amer. Ceram. Soc. **77**, 2505 (1994).

[2] E.A. Kotomin, A.I. Popov, and A. Stashans, J. Phys.: Condens. Matter **6**, L569 (1994).

[3] B.D. Evans, J. Nucl. Mater. **219**, 202 (1995).

[4] E.A. Kotomin, A.I. Popov, and A. Stashans, Phys. Status Solidi B **207**, 69 (1998).

[5] E.A. Kotomin and A.I. Popov, Nucl. Instrum. Methods Phys. Res. B **141**, 1 (1998).

[6] J.T. Devreese, V.M. Fomin, E.P. Pokatilov, E.A. Kotomin, R.I. Eglitis, and Yu.F. Zhukovskii, Phys. Rev. B **63**, 184304 (2001).

[7] K. Matsunaga, T. Tanaka, T. Yamamoto, and Y. Ikuhara, Phys. Rev. B **68**, 085110 (2003).

[8] N.D.M. Hine, K. Frensch, W.M.C. Foulkes, and M.W. Finnis, Phys. Rev. B **79**, 024112 (2009).

[9] A.A. Sokol, A. Walsh, and C.R.A. Catlow, Chem. Phys. Lett. **492**, 44 (2010).

[10] A. Lushchik, Ch. Lushchik, K. Schwartz, F. Savikhin, E. Shablonin, A. Shugai, and E. Vasil'chenko, Nucl. Instrum. Methods Phys. Res. B **277**, 40 (2012).

[11] A. Platonenko, S. Piskunov, Yu.F. Zhukovskii, and E.A. Kotomin, IOP Conf. Ser.: Mater. Sci. Eng. **77**, 012001 (2015).

[12] Yu.F. Zhukovskii, A. Platonenko, S. Piskunov, and E.A. Kotomin, Nucl. Instrum. Methods B **374**, 29 (2016).

[13] E.A. Kotomin, V.N. Kuzovkov, A.I. Popov, and R. Vila, Nucl. Instrum. Methods B **374**, 107 (2016).

[14] E. Feldbach, E. Tõldsepp, M. Kirm, A. Lushchik, K. Mizohata, and J. Räisänen, Opt. Mater. (2016), in press: http://dx.doi.org/10.1016/j.optmat.2016.03.008.

[15] R. Dovesi, V.R. Saunders, C. Roetti, R. Orlando, C.M. Zicovich-Wilson, F. Pascale, B. Civalleri, K. Doll, N.M. Harrison, I.J. Bush, Ph. D'Arco, M.Llunell, M. Causá M, and Y. Noël, CRYSTAL14 User's Manual, University of Torino, 2014.

[16] A.D. Becke, J. Chem. Phys. **98**, 5648 (1993).

[17] J. Baima, A. Erba, M. Rérat, R. Orlando , and R. Dovesi, J. Phys. Chem. C **117**, 12864 (2013).

[18] M. Causá, R. Dovesi, and C. Roetti, Phys Rev B **43**, 11937 (1991).

[19] H.J. Monkhorst and J.D. Pack, Phys. Rev. B **13**, 5188 (1976).

[20] R.S. Mulliken, J. Chem. Phys. **23**, 1833 (1955).

[21] C.M. Zicovich-Wilson, M.L. San-Román, and A. Ramírez-Solís, J. Phys. Chem. C **114**, 2989 (2010).

